Modified Gravity (MOG) and its test on galaxy clusters

Theodorus M. Nieuwenhuizen, Andrea Morandi, Marceau Limousin

Monthly Notices
of the
ROYAL ASTRONOMICAL SOCIETY

MNRAS **476,** 3393–3398 (2018)
Advance Access publication 2018 February 14

doi:10.1093/mnras/sty380

Modified Gravity and its test on galaxy clusters

Theodorus M. Nieuwenhuizen,[1,2]★ Andrea Morandi[3] and Marceau Limousin[4]

[1]*Institute for Theoretical Physics, University of Amsterdam, Science Park 904, PO Box 94485, NL-1090 GL Amsterdam, the Netherlands*
[2]*International Institute of Physics, UFRG, Anel Viário da UFRN - Lagoa Nova, Natal - RN, 59064-741, Brazil*
[3]*Physics Department, University of Alabama in Huntsville, Huntsville, AL 35899, USA*
[4]*Aix Marseille Université, CNRS, LAM, Laboratoire d'Astrophysique de Marseille, Marseille, France*

Accepted 2018 February 9. Received 2018 February 9; in original form 2017 October 4

ABSTRACT

The MOdified Gravity (MOG) theory of J. Moffat assumes a massive vector particle which causes a repulsive contribution to the tensor gravitation. For the galaxy cluster A1689 new data for the X-ray gas and the strong lensing properties are presented. Fits to MOG are possible by adjusting the galaxy density profile. However, this appears to work as an effective dark matter component, posing a serious problem for MOG. New gas and strong lensing data for the cluster A1835 support these conclusions and point at a tendency of the gas alone to overestimate the lensing effects in MOG theory.

Key words: gravitation – gravitational lensing: strong.

1 INTRODUCTION

With the ongoing no-show of the WIMP and the axion, and the natural dark matter (DM) candidate, the neutrino, long ruled out [but not given up; see e.g. Nieuwenhuizen (2016)], the DM riddle is ripe for reconsideration. One option is that DM effects do not arise from some particle but from a deviation from Newton's law in the weak-gravity regime. Examples of modified gravity (MOG) theories are: Modified Newtonian Dynamics (MOND) (Milgrom 1983; Famaey & McGaugh 2012); Entropic Gravity (EG1) (Verlinde 2011), and Emergent Gravity (EG2) (Verlinde 2017), which appears to be MOND-like; so-called $f(R)$ theories (Sotiriou & Faraoni 2010; De Felice & Tsujikawa 2010); and MOG (Moffat 2005). It is thus important to test these theories as much as possible. In Nieuwenhuizen (2017) one of us investigates whether these theories achieve to explain lensing properties of a well-documented galaxy cluster, Abell 1689 (in short A1689). It stands out since it is large, heavy, and probably quite relaxed. Good data exist for the X-ray gas and its strong and weak lensing properties (Morandi et al. 2012). Within the often employed spherical approximation, the investigation reveals that MOND, EG1, MOG, and $f(R)$ theories fail to give proper account of the lensing data; by default this also applies to EG2. It is noted that MOND and EG1 may survive if additional cluster DM, like $\sim$1.9 eV neutrinos, is added. As to the spherical approximation, let us note that the axis ratio of the gas is $1.1 - 1.06$ (on the plane of the sky) and $1.5 - 1.3$ (along the line of sight), moving from the centre towards the X-ray boundary (Morandi et al. 2011). Triaxial studies of this cluster have more recently been conducted by Umetsu et al. (2015).

The reported failure of MOG invoked a reaction by Moffat and Zoolideh Haghighi (MZH) who conclude that acceleration data of the A1689 cluster fare well within MOG (Moffat & Haghighi 2016). Hodson & Zhao (2017), on the other hand, seek to change MOND to incorporate an extra effect in clusters, and also compare to EG and MOG.

Because of the high stakes of the issue, we return here to the situation within the spherical approximation. Our reaction involves several points. First of all, it goes without saying that if the MOG acceleration predictions indeed fit the measurements while lensing data fail to do so, MOG remains a problematic theory. Secondly, to the best of our knowledge, there does not exist explicit acceleration data for A1689. The data points of fig. 2 of Nieuwenhuizen (2017) are estimates, and partly upper estimates, for the acceleration in theories, such as MOG, where light moves in the gravitational potential (Nieuwenhuizen 2017). The vanishing of the MZH acceleration at small radii in their fig. 1 is perfectly physical while consistent with the finite value of their upper bound. Thirdly, MZH employ A1689 parameters from our paper, Nieuwenhuizen (2017), in particular from two runs of X-ray data by the *Chandra* satellite that were introduced by us in Nieuwenhuizen & Morandi (2011). Below we present here the final A1689 *Chandra* data for the X-ray gas, and notice a calibration error in analysing the previous data sets. Hence, the gas fits must be redone; the implication for MOG will be presented below.

We also present new gas and strong lensing (SL) data for a second, well-relaxed cluster, A1835, and analyse them in a similar fashion.

In Section 2 we describe the final *Chandra* data for A1689 and new gas data for A1835, and fit them to analytical formulas. We also present new SL data for both clusters. In Section 3 we recall some relations between observables. In Section 4 we present MOG theory and in Section 5 the comparison with the A1689 and A1835 data. We close with a discussion.

★ E-mail: t.m.nieuwenhuizen@uva.nl

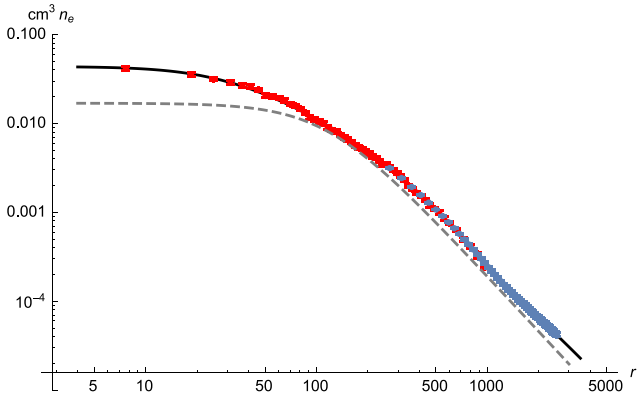

Figure 1. Data for the electron density n_e in A1689 from *Chandra* (red) and *ROSAT* (blue), with the analytic fit of equations (1), (3), (4), and (5) (full line). Dashed line: the β-model of Brownstein & Moffat (2006).

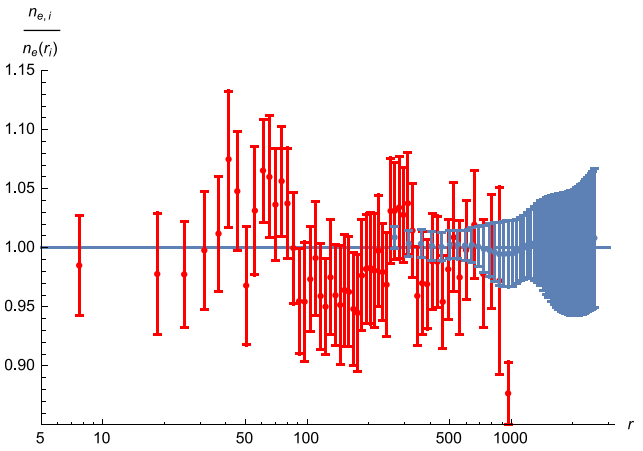

Figure 2. The data for n_e of Fig. 1 relative to the fit. Except for the outlying last *Chandra* point, nearly all points lie within one standard deviation from the fit.

2 DATA DESCRIPTION

2.1 Abell 1689

All our results are scaled to the flat Λ cold dark matter cosmology with $\Omega_M = 0.3$, $\Omega_\Lambda = 0.7$, and a Hubble constant $H_0 = 70\,h_{70}$ km s^{-1} Mpc with $h_{70} = 1$. At the redshift $z = 0.183$ of the A1689 cluster, 1 arcsec corresponds to 3.076 kpc.

2.1.1 *Data for the X-ray gas*

We present the final data of the *Chandra* X-ray Observatory. The data reduction was carried out using the CIAO 4.8.1 and HEASOFT 6.19 software suites, in conjunction with the *Chandra* calibration data base (CALDB) version 4.7.2. Fig. 1 exhibits the resulting 56 data *Chandra* points at radii between 7.7 and 963 kpc.

Let us recall some properties of the X-ray gas. We adopt a typical $Z = 0.3$ solar metallicity for A1689, so that to a good approximation $n_p = 11\,n_\alpha$. With elements heavier than He neglected and 25 per cent of the gas weight in He, this implies that $n_e = (13/11)n_p$. The particle density is $n_e + n_p + n_\alpha = (25/13)n_e$ and hence the thermal pressure $p_g = (25/13)n_e k_B T_g$. The mass density reads $\rho_g = m_N n_p + 4m_N n_\alpha = (15/11)m_N n_p$, so $\rho_g = \overline{m}_N n_e$ with $\overline{m}_N = (15/13)m_N = 1.154\,m_N$. The mean molecular weight in $p = \rho_g k_B T/\mu m_N$ is $\mu = 3/5$. These factors agree within per mille with $n_e + n_{ion} = 1.9254\,n_e$ and $\mu = 0.5996$ from the solar abundance tables of Asplund et al. (2009).

Further data for n_e have been obtained from the *ROSAT* satellite with its Position Sensitive Proportional Counters (PSPC) camera (Eckert et al. 2012a). A resulting set of 50 'parametric' data points for n_p is publicly available (Eckert et al. 2012a,b). As r_i-values we take the mids of their bins. As seen in Figs 1 and 2, the *Chandra* and PR data sets overlap within their error bars for radii between 268 and 872 kpc (except for the outlying last *Chandra* point).

2.1.2 *Fit to the X-ray gas data in A1689*

The Sérsic mass profile $\rho = \rho_0 \exp[-(r/R_g)^{1/n_g}]$ gave inspiration for a cored Sérsic electron density profile (Nieuwenhuizen 2016),

$$n_S(r) = n_e^0 \exp\left[k_g - k_g\left(1 + \frac{r^2}{R_g^2}\right)^{1/(2n_g)}\right]. \quad (1)$$

The best fit of this profile to the final *Chandra* data gives $\chi^2/\nu = 0.692$ for all 56 points included (so that the number of degrees of freedom is $\nu = 52$) and $\chi^2/\nu = 0.504$ when the outlying last point is discarded, which we do from now on. The best fit for the latter case is (as expected, both cases coincide within the error bars)

$$n_e^0 = 0.0431 \pm 0.0017\,\mathrm{cm}^{-3}, \quad k_g = 2.50 \pm 0.36,$$
$$R_g = 24.6 \pm 2.9\,\mathrm{kpc}, \quad n_g = 3.32 \pm 0.21. \quad (2)$$

The statistics of the final *Chandra* data is better than for the two runs we employed before; even though the error bars are smaller, the χ^2 value becomes noticeably smaller. Nevertheless, the fit (2) does not get essentially smaller error bars; we attribute this to non-sphericalities in the cluster. But do notice that the value of n_e^0 in (2) is a factor of 1.5 smaller than the value employed in our earlier works due to a calibration error there. This new value for n_e^0 will shift our previous fits, but appear to have no qualitative impact for MOG or other theories.

The cored Sérsic profile has a stretched exponential decay, matched by the inner data of *ROSAT*/PSPC, but the latter data extend beyond 1 Mpc, where they expose a slower decay. To model this, we consider two forms of a tail. First, the cored isothermal tail for the electron and mass densities,

$$n_T = \frac{d_t n_e^0}{r^2 + R_t^2}, \quad \rho_{g,T} = \overline{m}_N n_T = \frac{\sigma_g^2}{2\pi G(r^2 + R_t^2)}, \quad (3)$$

with $\sigma_g^2 = 2\pi G \overline{m}_N d_t n_e^0$, is combined with the Sérsic profile as

$$n_e(r) = \left(\frac{n_S^{s_t}(r) + n_T^{s_t}(r)}{1 + (d_t/R_t^2)^{s_t}}\right)^{1/s_t}, \quad (4)$$

so that $n_e(0) = n_e^0$. The fit leads to the very small $\chi^2(n_e)/\nu = 0.32$ and the parameters

$$n_e^0 = 0.04376 \pm 0.00098\,\mathrm{cm}^{-3}, \quad k_g = 2.06 \pm 0.12,$$
$$R_g = 21.8 \pm 1.4\,\mathrm{kpc}, \quad n_g = 3.044 \pm 0.062,$$
$$d_t = 6660 \pm 255\,\mathrm{kpc}^2, \quad \sigma_g = 476.5 \pm 7.7\,\mathrm{km\,s}^{-1},$$
$$R_t = 718 \pm 108\,\mathrm{kpc}, \quad s_t = 8.4 \pm 2.7. \quad (5)$$

The relative errors in these parameters are 0.022, 0.057, 0.062, 0.021, 0.038, 0.016, 0.15, and 0.32, respectively. Not all tail parameters are strongly constrained: R_t and s_t have appreciable errors.

One reason for this is that s_t is only determined by the few data in the cross over region from n_S to n_T. The fit for n_e is exposed in Figs 1 and 2. The ratios $n_{e,i}/n_e(r_i)$ are exposed in Fig. 2; they overlap nearly all within their error bars with the ideal value 1, causing the small $\chi^2(n_e)/\nu = 0.32$.

As a second model we consider the Burkert tail

$$n_T = \frac{d_t n_e^0 R_t}{(r + R_t)(r^2 + R_t^2)}. \tag{6}$$

Compared to the tail (3) it decays quicker and leads to an only logarithmically divergent gas mass. It respects the data points equally well, since it also achieves $\chi^2/\nu = 0.32$. The fit parameters are

$$\begin{aligned} n_e^0 &= 0.0438 \pm 0.0010\,\mathrm{cm}^{-3}, & k_g &= 2.04 \pm 0.12, \\ R_g &= 21.8 \pm 1.4, \mathrm{cm}^{-3}, & n_g &= 3.031 \pm 0.065, \\ d_t &= 22052 \pm 594\,\mathrm{kpc}^2, & R_t &= 1750 \pm 135\,\mathrm{kpc}, \\ s_t &= 4.9 \pm 1.1. \end{aligned} \tag{7}$$

The relative errors are here 0.023, 0.060, 0.063, 0.021, 0.027, 0.077, and 0.22, respectively.

The β-model $n_e(r) = n_e^0(1 + r^2/R_g^2)^{-3\beta/2}$ yields a considerably worst best fit, $\chi^2/n_{\rm bin} = 6.8$ with $n_e^0 = 0.0243 \pm 0.0010$, $R_g = 105.4 \pm 3.4$ kpc, and $\beta = 0.6701 \pm 0.0054$, having the small relative errors 0.043, 0.032, and 0.0080, despite the large χ^2. The β-model employed in Brownstein & Moffat (2006) has parameters $\rho_0 = 0.33\,10^{-25}\mathrm{gr\,cm}^{-3}$, corresponding to $n_e^0 = 0.0169\,\mathrm{cm}^{-3}$, $R_g = 114.8$ kpc, and $\beta = 0.690$. This leads to a truly bad fit indicated by $\chi^2/(55 + 50) = 85.1$, so this model can only be used with proper care. It is depicted by the dashed line in Fig. 1.

2.1.3 *Strong lensing in A1689*

The SL data arise from background galaxies lensed by the cluster. While a full *Einstein* ring does not occur, galaxies not-too-far from the sightline to the cluster centre are observed as an arclet or a set of $n \leq 7$ arclets in A1689. Its SL mass model was first derived in Limousin et al. (2007). From the arclets the computer code LENSTOOL, presented by Jullo et al. (2007) and Kneib et al. (2011), has now produced candidate maps for the $2-d$ mass distribution; this being an underdetermined problem, a set of maps, labelled by $\mu = 1, \cdots, \mathcal{N}$, can be generated. In total $\mathcal{N} = 1001$ solutions ('samples') have been achieved. These maps are integrated over circles around the centre to yield the $2d$ mass $\mathcal{M}_{2d}^{(\mu)}(r_n)$ within a cylinder of radius r_n. A number of $N = 149$ radii r_n are chosen such that the $\log r_n$ have uniform spacing 0.0380 between $r_1 = 3.15355$ kpc and $r_{149} = 876.783$ kpc. From each $\mathcal{M}_{2d}^{(\mu)}$ one gets $\overline{\Sigma}_n^{(\mu)} = \mathcal{M}_{2d}^{(\mu)}(r_n)/\pi r_n^2$. Summation over μ brings the statistical averages $M_{2d}(r) = (1/\mathcal{N})\sum_\mu \mathcal{M}_{2d}^{(\mu)}(r_n)$ and

$$\overline{\Sigma}_n = \frac{M_{2d}(r_n)}{\pi r_n^2} = \frac{1}{\mathcal{N}} \sum_\mu \overline{\Sigma}_n^{(\mu)}, \qquad (n = 1, \ldots, 149). \tag{8}$$

In shells without arclets, the LENSTOOL program produces constant values for M_{2d}, of which only the one at smallest r provides physical information. Hence not all r_n contain proper information about $\overline{\Sigma}_n$, but in total 117 of them do so (see Fig. 4).

We shall not consider related data for the line-of-sight mass density Σ, since they contain no new information. Moreover, to obtain them from $M_{2d}(r) = \pi r^2 \overline{\Sigma}(r) = 2\pi \int_0^r \mathrm{d}s\, s\Sigma(s)$, a numerical differentiation is needed, which introduces ambiguities.

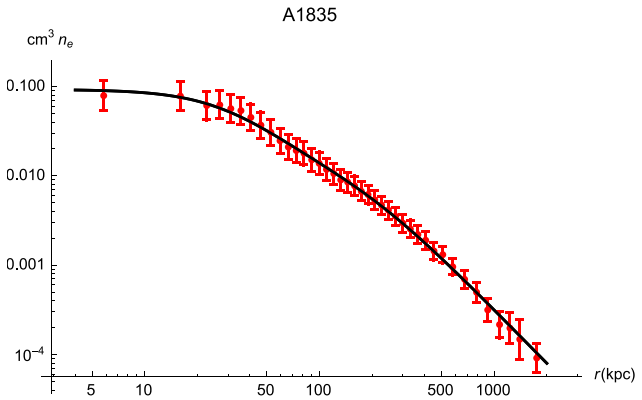

Figure 3. Data for n_e in A1835 and their best fit (10) with (11).

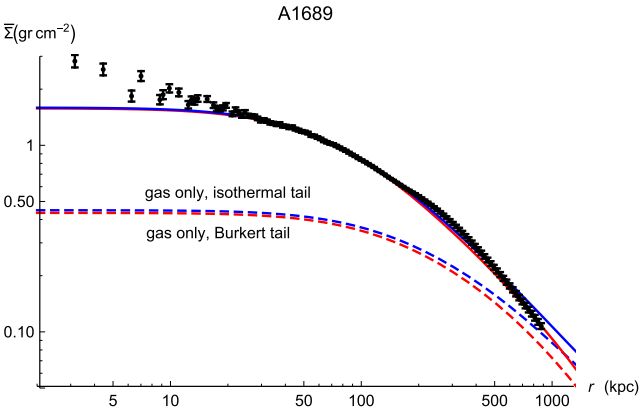

Figure 4. $\overline{\Sigma}(r)$ in A1689 in MOG theory. The dashed lines show the contribution of the X-ray gas, with isothermal tail (blue) or Burkert tail (red). The full lines exhibit the addition of the galaxy mass density in both cases. They mimic a DM component.

The correlations due to sample-to-sample variations are

$$\Gamma_{mn} = \frac{1}{\mathcal{N}} \sum_\mu [\overline{\Sigma}_m^{(\mu)} - \overline{\Sigma}_m][\overline{\Sigma}_n^{(\mu)} - \overline{\Sigma}_n]. \tag{9}$$

The standard estimate for the error bar in $\overline{\Sigma}_n$ is $\delta\overline{\Sigma}_n = (\Gamma_{nn})^{1/2}$; as usual in cases of correlated data, the full information on errors is coded in the covariance matrix Γ_{mn}.

2.2 Abell 1835

The cluster Abell 1835 is a massive cluster which shows several indications of a well-relaxed dynamical state. At its redshift $z = 0.253$, 3.947 kpc corresponds to 1 arcsec.

2.2.1 *The X-ray gas*

The setup for A1835 presented by two of us (Morandi et al. 2012) is followed. The data reduction is carried out using the CIAO 4.8.1 and HEASOFT 6.19 software suites, in conjunction with the *Chandra* calibration data base (CALDB) version 4.7.2. We measure the emission measure profile EM $\propto \int n_e^2 \mathrm{d}l$ from the X-ray images. The radial EM profile is derived with the vignetting correction and direct subtraction of the Cosmic X-ray Background (CXB)+particle+readout artefact background. For the particle background modelling, we use the scaled stowed background. In order to measure the CXB, we

used the regions free of the source emission. We then deprojected the measured temperature and EM profiles in order to infer the gas density profiles.

A set of 40 data points $(r_i, n_{\mathrm{e},i}, \delta n_{\mathrm{e},i})$ for the electron density has been produced. The errors $\delta n_{\mathrm{e},i}$ are larger than in the A1689 case, and constrain the fit profiles less well. We find that the following profile explains the data well:

$$n_{\mathrm{e}}(r) = n_{\mathrm{e}}^0 \frac{1 + r^2/R_0^2}{(1 + r^2/R_1^2)(1 + r^2/R_2^2)}. \tag{10}$$

The best fit has parameters

$$n_{\mathrm{e}}^0 = 0.0927 \pm 0.0070\,\mathrm{cm}^{-3}, \quad R_0 = 91 \pm 13\,\mathrm{kpc},$$
$$R_1 = 31.8 \pm 2.9\,\mathrm{kpc}, \quad R_2 = 169 \pm 15\,\mathrm{kpc}. \tag{11}$$

It has $\nu = 40 - 4$ degrees of freedom and $\chi^2/\nu = 0.0778$. This stunningly low value reflects that the fit goes through nearly all data points, in the presence of the somewhat large error bars (see Fig. 3).

With $\sigma_{\mathrm{g}}^2 = 2\pi G \overline{m}_N n_{\mathrm{e}}^0 R_1^2 R_2^2/R_0^2$, the gas mass density may be written as

$$\rho_{\mathrm{g}} = \overline{m}_N n_{\mathrm{e}} = \frac{\sigma_{\mathrm{g}}^2}{2\pi G} \frac{r^2 + R_0^2}{(r^2 + R_1^2)(r^2 + R_2^2)}. \tag{12}$$

It has an isothermal decay $\rho_{\mathrm{g}} \approx \sigma_{\mathrm{g}}^2/2\pi G r^2$ with

$$\sigma_{\mathrm{g}} = 496.9 \pm 6.4\,\mathrm{km\,s}^{-1}. \tag{13}$$

2.2.2 *Strong lensing by A1835*

The SL data have been generated in the same way as for A1689. The selected radii have the same spacing 0.0380 on a logarithmic scale. The first radius is $r_1 = 4.027$ kpc and the last one is $r_{149} = 1120$ kpc. With again $\mathcal{N} = 1001$ samples, the averages $\overline{\Sigma}_n$ have been determined in the way described in Section 2.1.3. Also, here 117 of the r_n contain information.

3 LENSING OBSERVABLES

Because the background galaxies are far removed from the cluster, the lensing effects can be thought of as occurring due to mass projected on to the plane through the cluster centre. One studies the $2d$ mass $\mathcal{M}_{2d}$, that is, the mass contained in a cylinder of radius r around the sightline. Its average over the disc is $\overline{\Sigma}(r) = \mathcal{M}_{2d}(r)/\pi r^2$. This quantity can be expressed in terms of the $3d$ mass density,

$$\overline{\Sigma}(r) = \frac{4}{r^2}\int_0^r \mathrm{d}s\, s^2 \rho(s) + \int_r^\infty \mathrm{d}s\, \frac{4s\rho(s)}{s + \sqrt{s^2 - r^2}}. \tag{14}$$

In MOG $\mathcal{M}_{2d}$ is an effective mass and ρ an effective mass density. In general, $\overline{\Sigma}$ can be expressed in terms of the gravitational potential φ as (Nieuwenhuizen 2009)

$$\overline{\Sigma}(r) = \frac{1}{\pi G}\int_0^\infty \mathrm{d}s\, \varphi'(r\cosh s). \tag{15}$$

This expression holds not only for general relativity but for any theory in which light moves in the gravitational potential or, at least, does so in the first post-Newtonian approximation. In particular, it applies to MOG.

4 MODIFIED GRAVITY

The MOG theory of J. Moffat aims to replace DM by a modification of Newton's law (Moffat 2006). Next to the standard tensor field, there is a massive vector field, which adds a repulsive term to the gravitational potential. In MOG the potential reads

$$\begin{aligned}\varphi &= -G\int \mathrm{d}^3 r' \frac{\rho_m(\boldsymbol{r}')}{|\boldsymbol{r} - \boldsymbol{r}'|}\left(\alpha + 1 - \alpha e^{-\mu|\boldsymbol{r}-\boldsymbol{r}'|}\right)\\ &= (\alpha+1)\varphi_N + \alpha\varphi_V\end{aligned} \tag{16}$$

with the subscript N denoting 'Newton' and V 'vector'. α is a dimensionless parameter relating the strength of the tensor field to Newton's constant G and μ is the inverse range of the vector field. A fit to galaxy catalogues yields $\alpha = 8.89 \pm 0.34$ and $\mu = 0.042 \pm 0.004\,\mathrm{kpc}^{-1}$ (Moffat & Rahvar 2013). These errors are small enough to have no influence on our conclusions determined by the central values.

The separate parts of the potential satisfy the massless and massive Poisson equations, respectively,

$$\nabla^2\varphi_N = 4\pi G\rho_m, \tag{17}$$

$$\nabla^2\varphi_V - \mu^2\varphi_V = -4\pi G\rho_m. \tag{18}$$

In the philosophy that only baryonic matter exists, the matter density consists of galaxies and X-ray gas,

$$\rho_m = \rho_{\mathrm{G}} + \rho_{\mathrm{g}}. \tag{19}$$

In case of spherical symmetry we may introduce

$$J(r) = 4\pi G\, r\rho_m(r), \tag{20}$$

and derive the explicit expressions

$$\begin{aligned}\varphi(r) = &-\int_0^r \mathrm{d}u \left[(\alpha+1)u - \frac{\alpha}{\mu}e^{-\mu r}\sinh\mu u\right]\frac{J(u)}{r}\\ &-\int_r^\infty \mathrm{d}u \left[(\alpha+1)r - \frac{\alpha}{\mu}e^{-\mu u}\sinh\mu r\right]\frac{J(u)}{r}.\end{aligned} \tag{21}$$

Here, the terms proportional to $\alpha + 1$ are Newtonian, while the ones proportional to α are derived by writing equation (18) as $(r\varphi_V)'' - \mu^2 r\varphi_V = -J(r)$ and employing the Greens function $\exp(-\mu r_>)(\sinh\mu r_<)/\mu$, where $r_< = \min(r, u)$ and $r_> = \max(r, u)$. As it should, employing the decomposition (16), equation (21) may be checked from equations (17) and (18).

For large r it follows that (Moffat 2006)

$$\begin{aligned}\varphi(r) &\approx (\alpha+1)\phi_N(r) + \frac{4\pi\alpha G}{\mu^2}\rho_m(r)\\ &\approx (\alpha+1)\phi_N(r).\end{aligned} \tag{22}$$

The acceleration is inwards and has magnitude

$$\begin{aligned}\varphi'(r) = &\frac{\alpha+1}{r^2}\int_0^r \mathrm{d}u\, u J(u)\\ &-\frac{\alpha}{\mu r^2}(1+\mu r)e^{-\mu r}\int_0^r \mathrm{d}u\, \sinh\mu u\, J(u)\\ &+\frac{\alpha}{\mu r^2}(\mu r\cosh\mu r - \sinh\mu r)\int_r^\infty \mathrm{d}u\, e^{-\mu u} J(u).\end{aligned} \tag{23}$$

Its small-r behaviour reads $\varphi'(r) = Cr$ with

$$C = \frac{4\pi G}{3}\left[\rho_m(0) + \alpha\mu^2\int_0^\infty \mathrm{d}u\, e^{-\mu u}\, u\, \rho_m(u)\right], \tag{24}$$

which is non-Newtonian since the second term is non-zero. It will only be small if the range of ρ is much smaller than $1/\mu$, like for stars and their planetary systems.

5 MOG APPLIED TO CLUSTERS

5.1 A large set of clusters

A set of 11 clusters is analysed in Moffat & Rahvar (2014) and a set of 106 clusters in Brownstein & Moffat (2006). Gas is modelled by β-profiles (not necessarily an optimal fit; see Fig. 1) while hydrostatic equilibrium is assumed (now known to be often violated in the outskirts). Most of these clusters are non-relaxed, non-spherical, and not well documented, e.g. lacking data for the X-ray gas. With the resulting model parameters not well constrained, these fits can at best be indicative. Conclusive indications must necessarily derive from well-constrained cases.

5.2 Abell 1689

We first consider the application to A1689. The new $\overline{\Sigma}$ data with their error bars taken from the diagonal elements of the covariance matrix are presented in Fig. 4. The MOG contribution of the new X-ray gas data alone, that is, of the gas in the absence of galaxies, is depicted by the dashed lines in Fig. 4, corresponding to the isothermal and Burkert tails, respectively. It is seen that MOG predicts approximately the proper strength for $\overline{\Sigma}$ at $r \sim 1$ Mpc, but deviates quickly at lower r. To achieve a matching of the data, a tentative fit for the galaxy distribution, inspired by the one of Limousin et al. (2007), is provided by

$$\rho_{\rm G} = \frac{6(1+r^2/R_0^2)}{(1+r^2/R_1^2)(1+r^2/R_2^2)(1+r^2/R_3^2)^{0.4}}\,\frac{m_N}{\rm cm^3}, \tag{25}$$

with $\{R_0, R_1, R_2, R_3\} = \{10, 4, 15, 130\}$ kpc. Its effect on $\overline{\Sigma}$ is presented in Fig. 4. Its slow decay factor $(1+r^2/R_3^2)^{-0.4}$ expresses that this $\rho_{\rm G}$ tries to use the galaxy distribution as an effective a DM component, a behaviour that goes against the philosophy of MOG and was encountered previously (Nieuwenhuizen 2017). The mass in galaxies is $5.3 \times 10^{12}{\rm M}_\odot$ within 100 kpc and further $2.2 \times 10^{13}{\rm M}_\odot$ between 100 kpc and 1 Mpc, while the gas mass is $8.0 \times 10^{13}{\rm M}_\odot$ in the latter domain. Fits with such a fraction of baryonic mass in galaxies are not acceptable, often the brightest cluster galaxy is considered to dominate the combined mass of the galaxies.

5.3 Abell 1835

The $\overline{\Sigma}$ data are presented in Fig. 5, together with the effect of the gas alone. A tentative match with the data is found for the galaxy mass density profile

$$\rho_{\rm G} = \frac{5.3\,(1+r^2/R_0^2)^2}{(1+r^2/R_1^2)^2(1+r^2/R_2^2)^2}\,\frac{m_N}{\rm cm^3}, \tag{26}$$

with

$$R_0 = 88\,{\rm kpc}, \quad R_1 = 11\,{\rm kpc}, \quad R_2 = 570\,{\rm kpc}. \tag{27}$$

The result is also presented in Fig. 5. Because R_2 is large, this profile again acts as a form of DM. The galaxies' mass is $2.0 \times 10^{12}\,{\rm M}_\odot$ within 100 kpc; there should still be $3.0 \times 10^{13}\,{\rm M}_\odot$ in galaxies between 100 kpc and 1 Mpc, to be compared with $9.2 \times 10^{13}{\rm M}_\odot$ in gas in that domain. Such a large fraction of bayrons in galaxies is unrealistic.

In the large r domain ($r > 700$ kpc) the gas already produces a larger $\overline{\Sigma}$ than deduced from the lensing alone; this impossibility is indeed worrisome because of the different trends, so that intersection between data and the gas contribution must occur. Fig. 5

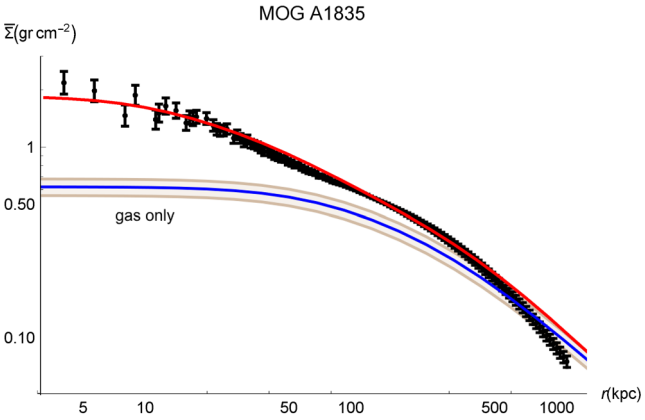

Figure 5. $\overline{\Sigma}(r)$ in MOG theory. The lower lines show the contribution of the X-ray gas with $1-\sigma$ error bars. The upper line exhibits the additional effect of the galaxy mass density. It mimics a DM component.

exhibits this behaviour for the best gas fit, with a 1σ error band in the amplitude. A similar but less pronounced behaviour is present for A1689 with an isothermal tail to the gas data (see Fig. 4). The present data thus point at a serious problem for MOG. From the anti-MOG, pro-DM perspective, it may simply express that MOG's large r enhancement factor with respect to baryons, $\alpha + 1 = 9.9$, should not replace the standard cosmic total-to-baryonic matter density ratio $\Omega_{\rm c}/\Omega_{\rm B} + 1 \approx 6.4$. This then implies that a large portion of the mass is still missing, and this necessitates a component of hidden baryons or DM in the cluster core and outskirts.

5.4 Further aspects of MOG

Let us speculate on other aspects of MOG. Larger values of μ have been employed. Moffat & Haghighi (2016), e.g. also consider $\mu = 0.125\,{\rm kpc}^{-1}$, while Martino & Laurentis (2017) investigate the scale dependence of μ and α. Taking a larger μ value at fixed r drives MOG further away from the Newton theory. For smooth mass distributions, the small-r coefficient (24) will converge for large μ to the non-Newtonian form

$$\varphi'(r) \to \frac{4\pi G}{3}(\alpha+1)\rho_m(0), \tag{28}$$

in accord with (22) but likely problematic in practice.

The point-mass MOG potential

$$\varphi = -\frac{GM}{r}(1+\alpha-\alpha e^{-\mu r}) \tag{29}$$

will have the exponential vanishing in the application to satellite galaxies, and be again $\alpha + 1 \sim 10$ times stronger than the Newton potential. We do not expect that smearing of the mass distributions will compensate this effect.

6 CONCLUSION

We have presented new data sets for the X-ray gas density and SL effects of the well-studied cluster A1689 and the now accordingly investigated cluster A1835. These data sets are considered within MOG theory. It is found that the gas alone matches the lensing property $\overline{\Sigma}(r) = M_{2d}(r)/\pi r^2$ around $r = 1$ Mpc. At smaller r an extra effect is needed. The demand of a mass density profile for the galaxies localized near the cluster centre appears to be in conflict with the demand that no DM is present. Fits tend to need matter

from galaxies far from the centre, where there exist not so many of them. There also exists a trend for the gas to already overshoot the lensing data at large r, in particular for A1835, which is physically impossible. On the scale of interacting satellite galaxies the gravitational potential seems to strongly overestimate the Newtonian value. These issues pose serious problems for the MOG theory.

ACKNOWLEDGEMENTS

The authors are grateful for the careful remarks and useful hints by the unknown referee. AM acknowledges support from *Chandra* grant GO415115X and NASA grants NNX14AI29G and NNX15AJ30G. ML acknowledges CNRS, CNES, and PNCG for support, the staff of the 'Cluster de calcul intensif HPC' Platform of the OSU Institut Pythéas (Aix-Marseille Université, INSU-CNRS) for providing computing facilities, and M. Libes and C. Yohia from the Service Informatique de Pythéas (SIP) for technical assistance.

REFERENCES

Asplund M., Grevesse N., Sauval A. J., Scott P., 2009, ARA&A, 47, 481
Brownstein J., Moffat J., 2006, MNRAS, 367, 527
De Felice A., Tsujikawa S., 2010, Living Rev. Relativ., 13, 1002
Eckert D. et al., 2012a, A&A, 541, A57
Eckert D. et al., 2012b, available at: http://www.isdc.unige.ch/~deckert/newsite/The_Planck_ROSAT_project.html
Famaey B., McGaugh S. S., 2012, Living Rev. Relativ, 15, 10
Hodson A. O., Zhao H., 2017, preprint (arXiv:1703.10219)
Jullo E., Kneib J.-P., Limousin M., Eliasdottir A., Marshall P., Verdugo T., 2007, New J. Phys., 9, 447
Kneib J.-P., Bonnet H., Golse G., Sand D., Jullo E., Marshall P., 2011, Astrophysics Source Code Library
Limousin M. et al., 2007, ApJ, 668, 643
Martino I. D., Laurentis M. D., 2017, Phys. Lett. B, 770, 440
Milgrom M., 1983, ApJ, 270, 371
Moffat J., 2005, J. Cosmol. Astropart. Phys., 2005, 003
Moffat J. W., 2006, J. Cosmol. Astropart. Phys., 2006, 004
Moffat J., Haghighi M., 2016, preprint (arXiv:1611.05382)
Moffat J., Rahvar S., 2013, MNRAS, 436, 1439
Moffat J. W., Rahvar S., 2014, MNRAS, 441, 3724
Morandi A., Limousin M., Rephaeli Y., Umetsu K., Barkana R., Broadhurst T., Dahle H., 2011, MNRAS, 416, 2567
Morandi A. et al., 2012, MNRAS, 425, 2069
Nieuwenhuizen T. M., 2009, Europhys. Lett., 86, 59001
Nieuwenhuizen T. M., 2016, J. Phys. Conf. Ser., 701, 012022
Nieuwenhuizen T. M., 2017, Fortschritte der Physik, 65, 1600050
Nieuwenhuizen T. M., Morandi A., 2011, J. Cosmol., 15, 6004
Sotiriou T. P., Faraoni V., 2010, Rev. Modern Phys., 82, 451
Umetsu K. et al., 2015, ApJ, 806, 207
Verlinde E., 2011, J. High Energy Phys., 2011, 1
Verlinde E., 2017, SciPost Phys., 2, 016

This paper has been typeset from a TEX/LATEX file prepared by the author.